Progress In Electromagnetics Research, Vol. 149, 161–171, 2014

Breast Imaging Using Microwave Tomography with Radar-Based Tissue-Regions Estimation

Anastasia Baran[1, *], Douglas Kurrant[2], Amer Zakaria[1, 3], Elise Fear[2], and Joe LoVetri[1]

Abstract—Microwave tomography (MWT) and a radar-based region estimation technique are combined to create a novel algorithm for biomedical imaging with a focus on breast cancer detection and monitoring. The region estimation approach is used to generate a patient-specific spatial map of the breast anatomy that includes skin, adipose and fibroglandular regions, as well as their average dielectric properties. This map is incorporated as a numerical inhomogeneous background into an MWT algorithm based on the finite element contrast source inversion (FEM-CSI) method. The combined approach reconstructs finer structural details of the breast and better estimates the dielectric properties than either technique used separately. Numerical results obtained with the novel combined algorithmic approach, based on synthetically generated breast phantoms, show significant improvement in image quality.

1. INTRODUCTION

Biomedical imaging at microwave frequencies has shown potential in breast cancer detection and monitoring [1–3]. The potential advantages of microwave imaging over conventional modalities such as magnetic resonance imaging (MRI) and computed tomography (CT), are that it is relatively inexpensive and utilizes low power, non-ionizing radiation. Two techniques that exploit imaging at microwave frequencies are microwave tomography (MWT) and radar-based imaging.

Radar-based imaging uses ultra wideband pulses to illuminate the breast. Information is extracted from the backscattered energy that shows the location of strong scatterers such as a tumour [4] or the fibroglandular region in a heterogeneously dense breast. MWT measures the scattered field generated when the breast is illuminated with electromagnetic energy (usually single frequency time-harmonic waveforms). Iterative methods are applied to the data to solve an inverse scattering problem and reconstruct an "image" of the spatial distributions of the dielectric properties [5, 6].

These microwave methods have drawbacks that are challenging to overcome. In particular, both modalities have inherent limitations in *(i)* resolution of fine structures, particularly within the glandular region, and *(ii)* sensitivity to small and low contrast objects. Moreover, MWT has limitations in *(iii)* accuracy of recovered tissue properties [4, 7–9].

With both MWT and radar, the resolution of fine structures depends strongly on the frequencies of illumination. For a high resolution reconstruction using MWT, a large number of reconstruction elements are required to capture details related to the breast surface and the many spatially fine features of the interior structure. For typical MW measurement systems, the number of reconstruction elements far exceeds the number of independent data, leading to non-unique solutions that contribute to the ill-posedness of the problem and manifest as convergence to local minima. Consequently, tissue properties are inaccurately recovered leading to poor image quality.

Received 6 August 2014, Accepted 23 September 2014, Scheduled 14 October 2014

* Corresponding author: Anastasia Baran (umbarana@cc.umanitoba.ca).

[1] Department of Electrical and Computer Engineering, University of Manitoba, Winnipeg, MB R3T 5V6, Canada. [2] Department of Electrical and Computer Engineering, Schulich School of Engineering, University of Calgary, Calgary, Alberta T2N 1N4, Canada. [3] Amer Zakaria is now at the American University of Sharjah, Sharjah, United Arab Emirates.

Image quality, especially in terms of the accuracy of the recovered tissue properties, is also affected by the stability of the iterative inversion algorithm. Lack of numerical stability, a defining characteristic of ill-posed problems, affects any inversion technique's sensitivity to noise in the measurement data. The use of prior information about the electrical properties and anatomical structures of the imaged region, when incorporated into MWT biomedical inversion algorithms, helps to mitigate the problem of ill-posedness, significantly improving the quality of the reconstructed images [10–12]. For example, knowledge of the upper and lower bounds of the tissue properties is used in [9] to promote the spatial correlation of these parameters and to introduce a constraint into the optimization problem. This information is not patient-specific; it is derived from a general set of literature values, so stability is not fully realized. As discussed in [9], stability is achieved with the inclusion of additional regularization terms, but at the expense of reduced resolution of fine structures and a reduction in the sensitivity to small and low contrast objects. A patient-specific approach is proposed in [10] whereby a regularization technique introduces prior information extracted from MRI or x-ray CT modalities.

Introducing structural and dielectric prior information as an inhomogeneous background, which redefines the contrast for the inverse problem, can produce significant enhancements. For example, in [13] it was shown that using information about the fat thickness as an inhomogeneous background significantly improves the quality of the reconstructed images of human forearms [11, 13].

In this paper, we present a new approach to microwave imaging that uses patient-specific prior information derived using radar-based methods to improve the quality of the images reconstructed using MWT. A radar-based method segments the breast into regions dominated by skin, adipose and glandular tissues [14]. Mean values over these regions are estimated using a nonlinear optimization approach [15]. This patient specific information is incorporated as an inhomogeneous numerical background in a finite element contrast source inversion (FEM-CSI) algorithm [5]. The efficacy of the method is demonstrated using data generated from 2D numerical breast phantoms. The novel combined algorithmic approach to microwave imaging sets the stage for a feasible short-term experimental study as well as a longer term study which will be based on a future combined imaging system.

2. THE COMBINED ALGORITHM

2.1. Radar-Based Regional Imaging

The novel combined approach first utilizes a radar-based algorithm that segments the breast into a skin layer and regions dominated by adipose and glandular tissues as well as estimating the tissue properties in each of these regions [15]. The method uses UWB reflection data acquired with a monostatic scanning configuration whereby a co-located source/sensor is rotated to a number of equally spaced locations around the breast. The extent of each region is approximated by first determining points on the interfaces between the different regions. Contours are then fitted to these interface points. With the internal structure of the breast segmented, the mean dielectric properties over each region are estimated with a nonlinear optimization technique applied to the reflection data acquired by the monostatic scanning system. This segmentation and parameter estimation algorithm is described in [15]. The result of the radar-based method is a 2D spatial map, a regional permittivity map, that contains both geometric and dielectric information representing the breast's basic internal structure; this is used in the MWT algorithm to be described next.

2.2. Microwave Tomography

We assume a configuration for the microwave tomographic data collection based on the system described in [11]. In this configuration the MWT system collects single-frequency scattered field data with transmitting and receiving antennas in a circular chamber. The data are then inverted using the FEM-CSI algorithm described in [5]. This algorithm is an improvement on the standard FEM-CSI, shown in Fig. 1(a), as it allows one to incorporate prior information in the form of an inhomogeneous background containing known information about the dielectric properties and location of anatomical regions in the breast (Fig. 1(b)) [13]. In addition, the algorithm offers the benefit of performing inversion on triangular meshes, which can accommodate the irregular shapes of anatomical structures [5]. The

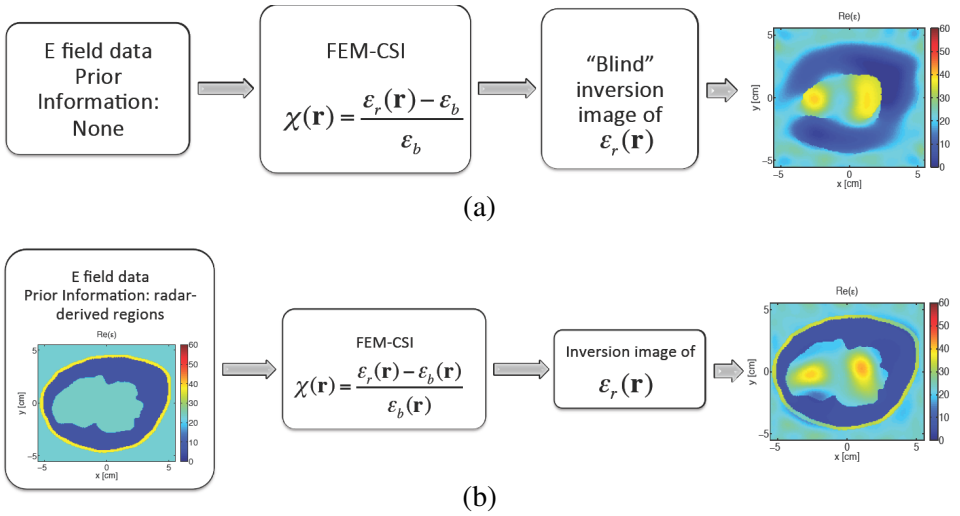

Figure 1. *Algorithm Flowchart*: (a) Standard FEM-CSI algorithm progression. (b) FEM-CSI algorithm including radar derived prior information.

FEM-CSI reconstructions are enhanced by the edge preserving multiplicative regularization described in [6].

2.3. Description of the Combined Approach

The combined approach is investigated for breast cancer imaging using numerical phantoms constructed on the basis of MRI images as discussed in [15]. In the combined algorithm, the breast's basic structural information is first extracted using the radar-based region estimation technique. The synthetic data for the geometric segmentation are collected with a 40 position monostatic scanning system whereby the antenna at each position is 10 mm from the breast surface. The breast is illuminated with an UWB differentiated Gaussian pulse having a −3 dB bandwidth of 4.14 GHz (1.45–5.59 GHz) — the frequency range of the antennas used in the University of Calgary's experimental system [4]. These reflection data are used to both segment the interior into regions and to estimate the mean dielectric properties over these regions. The synthetic data are all obtained using the FDTD technique. Furthermore, the backscattered fields are contaminated with a sequence of white Gaussian noise samples. The noise level is adjusted so that the signal-to-noise ratio (SNR) is 20 dB. The SNR in the time domain is defined as the ratio of the scattered-field energy to the energy of the added noise sequence.

Scattered data for the MWT algorithm are collected from the same phantoms using an FEM forward solver at a single frequency using 24 transmitting and receiving antennas equally distributed on a circle of 0.1 m radius. This scattered field is contaminated with 5% noise as described in [5], which corresponds to an SNR of just above 20 dB. The SNR in the frequency domain is commonly defined as the ratio of the average magnitude squared of the scattered field over all receiver locations to the average magnitude squared of the added noise. These data are independently inverted using MR-FEM-CSI to reconstruct the "blind" complex permittivity. These reconstructions are poor, but presented as a basis upon which to compare the images obtained via the combined approach.

For the combined approach, the complex permittivity of the segmented-regions, which are produced on a square grid, are transformed to the parameter space of the MR-FEM-CSI algorithm by interpolation onto a triangular mesh. This regional permittivity map is used as prior information in the form of a numerical inhomogeneous background, $\epsilon_b(\mathbf{r})$, for solving for the contrast, defined as

$$\chi(\mathbf{r}) = \frac{\epsilon(\mathbf{r}) - \epsilon_b(\mathbf{r})}{\epsilon_b(\mathbf{r})} \tag{1}$$

where $\mathbf{r}$ is the position vector and ϵ the complex permittivity of the unknowns. The reconstructions are obtained with the MR-FEM-CSI algorithm by inverting the same MWT scattered data. With this

formulation, the contrast values of all of the unknowns in the imaging domain are allowed to vary; they are not constrained by the geometry of the regional segmentation.

3. RESULTS

Results are presented for two separate cases at two different frequencies. The cases incorporate breast phantoms based on *model 2* and *model 3* described in [15]. In the first case, the phantoms are immersed in a water-glycerin solution having a complex relative permittivity of $23.3 - j23.4$ (similar to that used in [7]) and are illuminated by a 1 GHz incident field. In the second case, the surrounding fluid has a complex relative permittivity of $38 - j13$ (similar to that used in [16]) and the breast is radiated by a 2 GHz incident field. Note that the immersion media are not optimized for the particular breast phantoms being imaged. For the MWT reconstructions, we avoid an "inverse crime" by ensuring that the forward and inverse meshes are different. For this study, the radar-based regional maps are generated using air as an immersion medium, but the same results are obtainable in any medium.

The results are shown in Fig. 2, Fig. 3, Figs. 4 and 5, respectively. The numerical phantom is shown in subfigures (a), (b), and the blind MWT results in subfigures (c), (d). The radar-based region estimation results are shown in subfigures (e), (f), illustrating the definition of the regions dominated by skin, adipose and glandular tissues, as well as the average properties estimated for these regions. The information in (e) and (f) is used as prior information in the form of an inhomogeneous background in the FEM-CSI algorithm, resulting in the images shown in (g) and (h).

The improvement of the combined approach over the blind inversion is quantified by calculating the L_2 error norm:

$$L_2 = \frac{||\epsilon_{\text{phantom}}(\mathbf{r}) - \epsilon_{\text{recon}}(\mathbf{r})||_2}{||\epsilon_{\text{phantom}}(\mathbf{r})||_2}, \tag{2}$$

where $\epsilon_{\text{phantom}}$ and ϵ_{recon} are the complex permittivities of the phantom and MR-FEM-CSI reconstruction, and $\mathbf{r}$ is inside the phantom. These norms are calculated by interpolating the images onto uniform square grids of decreasing cell size until the norms converge — a technique described in [5]. The L_2 norms are listed in Table 1.

Table 1. L_2 norms for FEM-CSI reconstructions with and without radar-derived prior information.

Model Number	L_2 Blind Inversion	L_2 Prior Information
1-1, 1GHz	55.7%	49.6%
1-2, 1GHz	65.3%	71.3%
2-1, 2GHz	154.1%	48.7%
2-2, 2GHz	114.1%	72.5%

The complex permittivity is interpolated onto cross-sections for each case and presented in Fig. 6. The chosen cross-section, shown as the dashed line in Fig. 2(a) and Fig. 3(a), bisects the position of the tumour.

4. DISCUSSION

Reasonable blind inversion results are obtained for the 1 GHz cases, although the images are blurred. The blind inversion of case 1-2 shows difficulty in determining the edge of the breast, particularly in the real part of the reconstruction. In the 2 GHz cases, we observe a lack of convergence resulting in completely spurious images, which is quantified by the especially high L_2 norm. It is possible that this occurs because in this non-optimized immersion medium, the contrast between the matching media and the fat inside the breast is very high, making it difficult for the MR-FEM-CSI algorithm to find a reliable solution. Inaccurate recovery of the tissue properties and failure to resolve regional structures limits the diagnostic utility of these reconstructions.

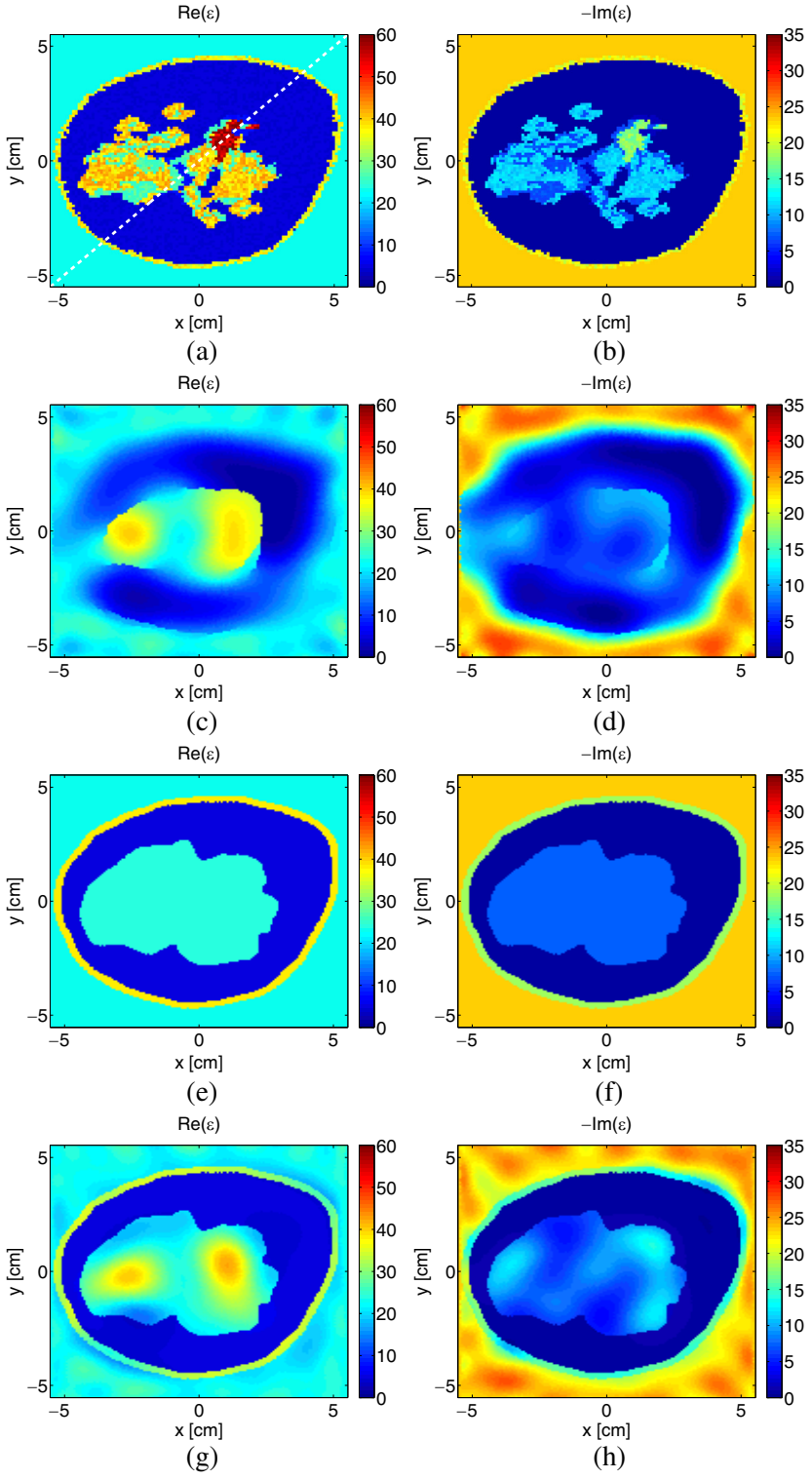

Figure 2. *Case 1-1, 1 GHz incident field:* (a) and (b): Real and imaginary parts of breast phantom. (c) and (d): Real and imaginary parts of MR-FEM-CSI reconstruction without prior information. (e) and (f): Real and imaginary parts of prior information obtained from radar-based imaging. (g) and (h): Real and imaginary parts of MR-FEM-CSI reconstruction with prior information.

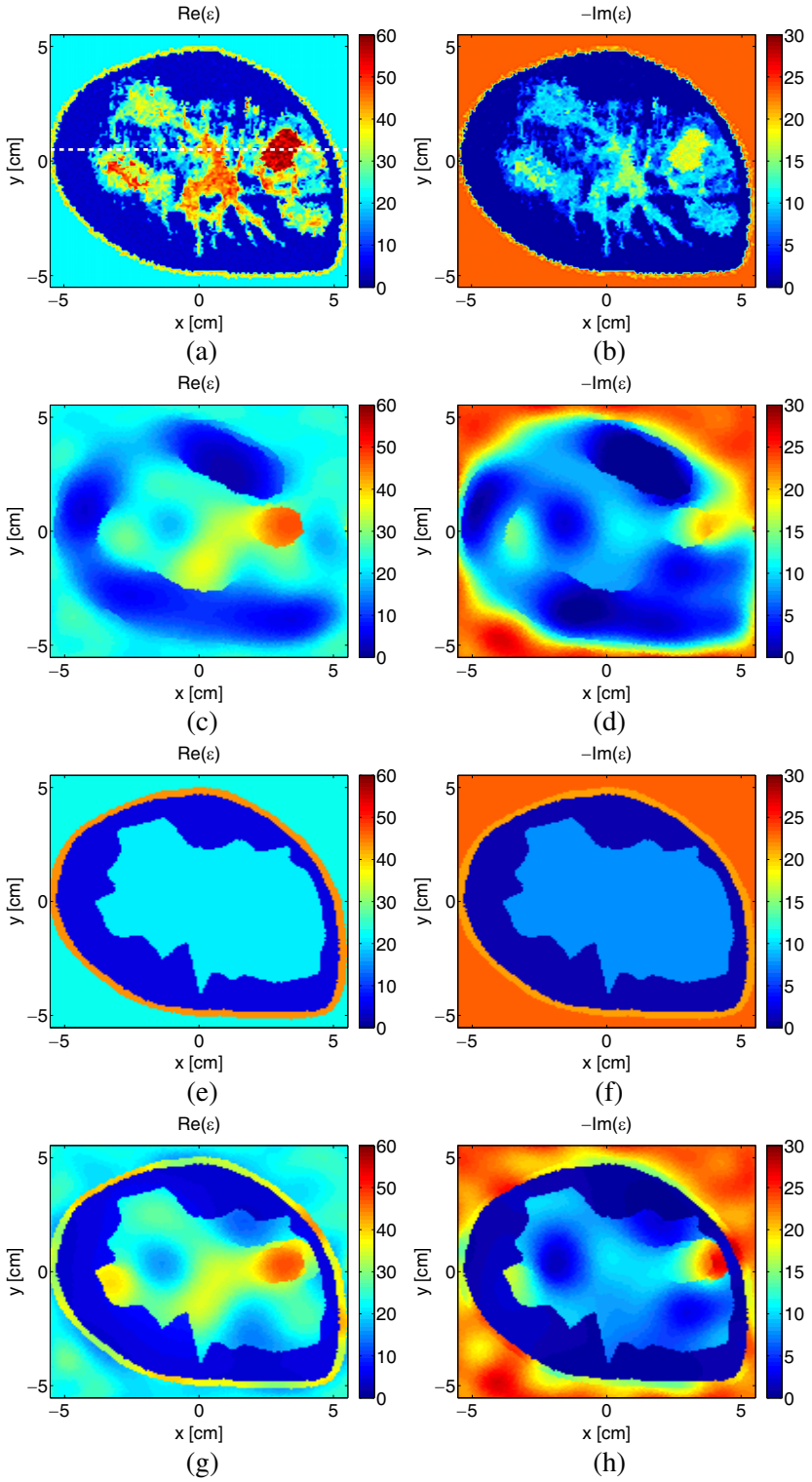

Figure 3. *Case 1-2, 1 GHz incident field*: (a) and (b): Real and imaginary parts of breast phantom. (c) and (d): Real and imaginary parts of MR-FEM-CSI reconstruction without prior information. (e) and (f): Real and imaginary parts of prior information obtained from radar-based imaging. (g) and (h): Real and imaginary parts of MR-FEM-CSI reconstruction with prior information.

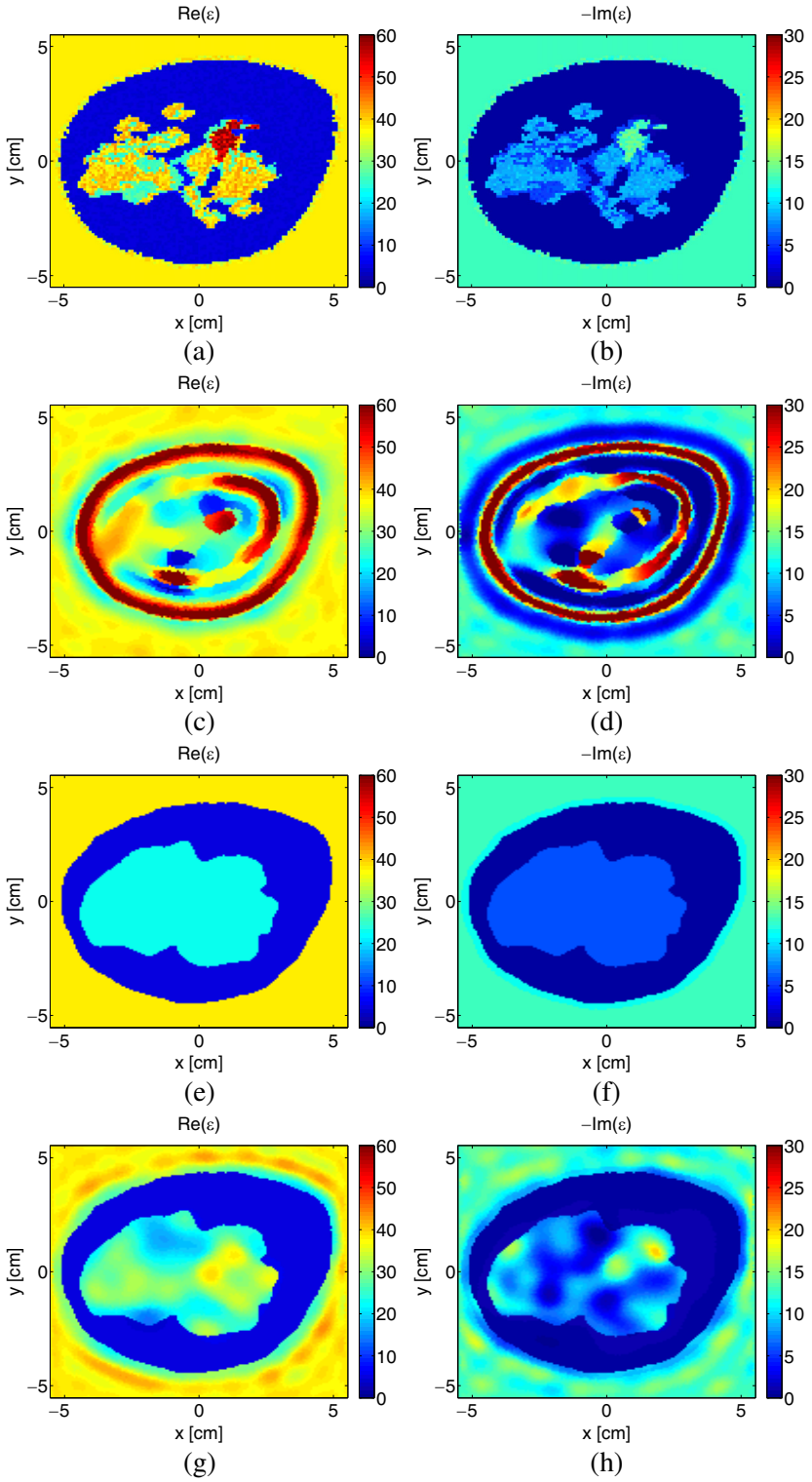

Figure 4. *Case 2-1, 2 GHz incident field*: (a) and (b): Real and imaginary parts of breast phantom. (c) and (d): Real and imaginary parts of MR-FEM-CSI reconstruction without prior information. (e) and (f): Real and imaginary parts of prior information obtained from radar-based imaging. (g) and (h): Real and imaginary parts of MR-FEM-CSI reconstruction with prior information.

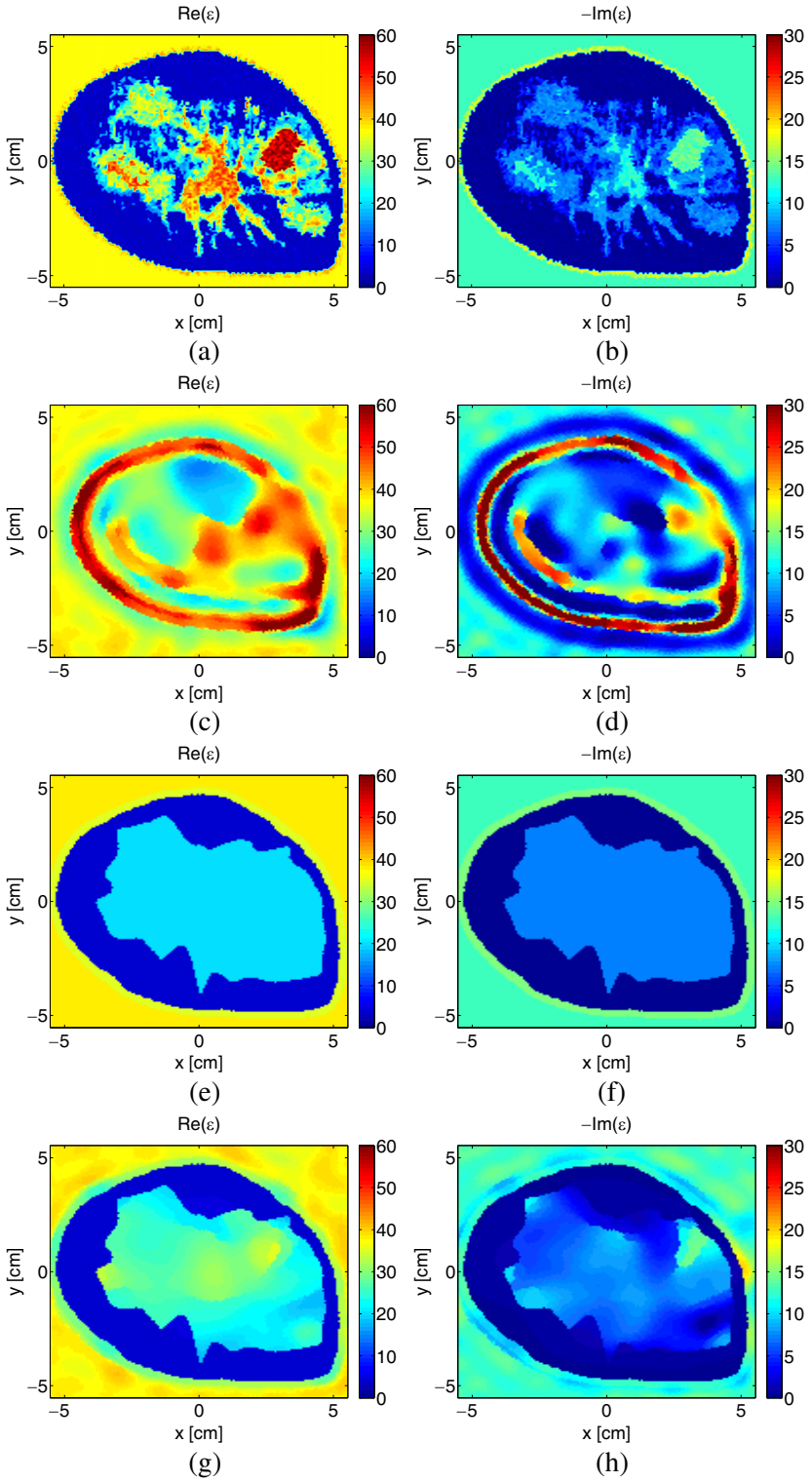

Figure 5. *Case 2-2, 2 GHz incident field*: (a) and (b): Real and imaginary parts of breast phantom. (c) and (d): Real and imaginary parts of MR-FEM-CSI reconstruction without prior information. (e) and (f): Real and imaginary parts of prior information obtained from radar-based imaging. (g) and (h): Real and imaginary parts of MR-FEM-CSI reconstruction with prior information.

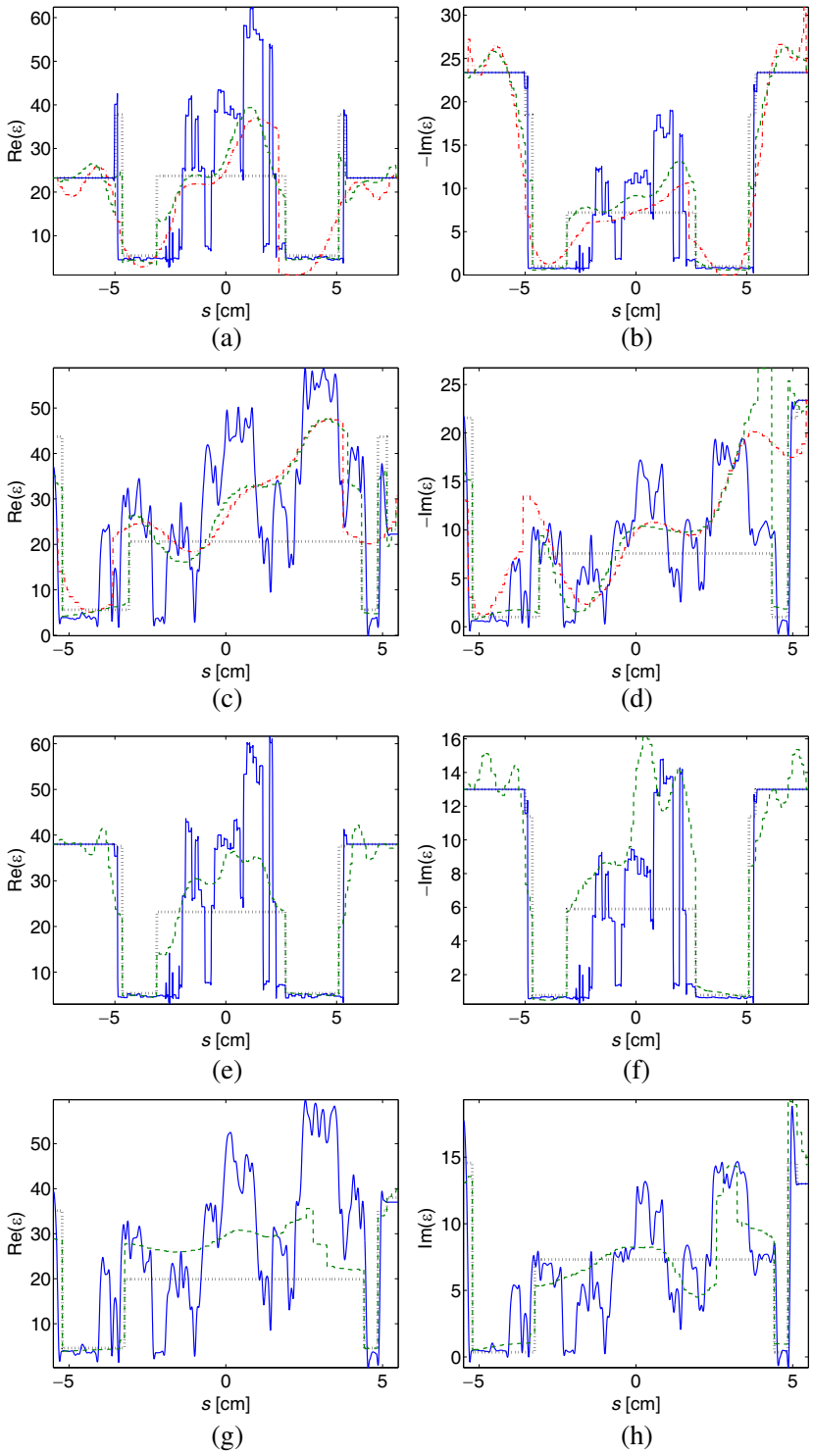

Figure 6. *Cross Sections*: Real and imaginary cross sections of case 1-1 ((a) and (b)), case 1-2 ((c) and (d)), case 2-1 ((e) and (f)) and case 2-2 ((g) and (h)) of images that bisect the tumour. Here s is the distance in cm, the blue solid line represents the phantom, the black line represented by bars is the regional reconstruction, the red line represented by '−.' is the blind inversion and the green dashed line is the reconstruction with prior information. Note the blind inversion results are not included at 2 GHz as they are unstable.

Use of the combined approach produces a substantial improvement in the accuracy and resolution of the reconstructions for cases 1-1, 2-1 and 2-2. The radar-based region-estimation technique provides a good estimation of the boundaries of the different regions but provides no information regarding the finer details within the fibroglandular region, including the existence of the tumour. With the combined approach, details within the fibroglandular region are now observable. This improvement is quantified by a decrease in L_2 for these cases. For cases 2-1 and 2-2, which are obtained at a higher frequency, the blind reconstructions are unstable. Use of the combined method provides a stable solution. For case 2-1 the tumour presence is now resolved, and the reconstructed dielectric properties approach the values of the known tissues. Scattered areas of adipose tissue within the fibroglandular region are also resolved. Case 2-2 does not conclusively reconstruct the tumour in either the real or imaginary parts. Imaging improvements are more clearly evident in the cross-sectional plots (Fig. 6).

For case 1-1, the combined method shows variations in the fibroglandular region that are consistent with the known structure of the tissue, and recovers the properties of the different tissue types more accurately than blind reconstruction. Case 1-2 is the only case considered that does not show a decrease in L_2 using the combined method, likely due to the fact that the dielectric properties of the tumour are overestimated in the imaginary part. Despite the increase in L_2, using the combined method provides us with more useful diagnostic information. The edge of the fibroglandular region is known, supporting the detection of a tumour, as they are typically found within the fibroglandular region of the breast. The tumour, which was previously undetectable in the imaginary part of the blind inversion, now becomes visible. Unfortunately, it also spreads to regions outside the breast. Future work will remove unknowns exterior to the breast by limiting the imaging domain to the region bounded by the skin. Preliminary results show that this improves reconstructions. The use of new image evaluation metrics, which apply to local geometries of interest, will better quantify improvements in these types of reconstructions.

In addition, the combined approach is much more robust with respect to the choice of immersion medium. We show inversion results at 1 GHz and 2 GHz with immersion media varying in both their real and imaginary permittivity values, and we have had success inverting at frequencies up to 4 GHz. Although the resolution and accuracy of the images varies, all cases resulted in substantially improved reconstructions. This "regularization" feature is especially advantageous as it may reduce the sensitivity to the immersion medium being used, allowing more options for clinical systems. The capacity to image at multiple frequencies also allows the possibility of incorporating all of the frequency information in the reconstruction process, providing more information for the MWT inversion.

5. CONCLUSION

We have presented a combined radar-MWT technique that incorporates radar-derived regional tissue maps as a numerical inhomogeneous background into an FEM-CSI MWT algorithm. This combined algorithm increases the quality of the images and provides more useful diagnostic information than either method used alone and has the added benefit of obtaining stable solutions where the traditional FEM-CSI is unable to do so. This method is robust and is able to reconstruct stable solutions from data collected at different frequencies, and using different immersion media, even if they are not necessarily optimized for breast imaging. Future work will include an investigation of appropriate frequency ranges for tumour detection, as well as an extension of the presented algorithm to 3D.

ACKNOWLEDGMENT

This project has been made possible through a grant from the Canadian Breast Cancer Foundation — Prairies/NWT Region.

REFERENCES

1. Meaney, P. M., M. W. Fanning, T. Raynolds, C. J. Fox, Q. Fang, C. A. Kogel, S. P. Poplack, and K. D. Paulsen, "Initial clinical experience with microwave breast imaging in women with normal mammography," *Academic Radiology*, Vol. 14, No. 2, 207–218, 2007.

2. Poplack, S. P., T. D. Tosteson, W. A. Wells, B. W. Pogue, P. M. Meaney, A. Hartov, C. A. Kogel, S. K. Soho, J. J. Gibson, and K. D. Paulsen, "Electromagnetic breast imaging: Results of a pilot study in women with abnormal mammograms," *Radiology*, Vol. 243, No. 2, 350–359, 2007.
3. Lazebnik, M., D. Popovic, L. McCartney, C. B. Watkins, M. J. Lindstrom, J. Harter, S. Sewall, T. Ogilvie, A. Magliocco, T. M. Breslin, et al., "A large-scale study of the ultrawideband microwave dielectric properties of normal, benign and malignant breast tissues obtained from cancer surgeries," *Physics in Medicine and Biology*, Vol. 52, No. 20, 6093, 2007.
4. Fear, E., J. Bourqui, C. Curtis, D. Mew, B. Docktor, and C. Romano, "Microwave breast imaging with a monostatic radar-based system: A study of application to patients," *IEEE Transactions on Microwave Theory and Techniques*, 2119–2128, 2013.
5. Zakaria, A., C. Gilmore, and J. LoVetri, "Finite-element contrast source inversion method for microwave imaging," *Inverse Problems*, Vol. 26, No. 11, 115010, 2010.
6. Zakaria, A. and J. LoVetri, "Application of multiplicative regularization to the finite-element contrast source inversion method," *IEEE Transactions on Antennas and Propagation*, Vol. 59, No. 9, 3495–3498, Sep. 2011.
7. Grzegorczyk, T. M., P. M. Meaney, P. A. Kaufman, R. M. di Florio-Alexander, and K. D. Paulsen, "Fast 3-d tomographic microwave imaging for breast cancer detection," *IEEE Transactions on Medical Imaging*, Vol. 31, No. 8, 1584–1592, 2012.
8. Nikolova, N. K., "Microwave imaging for breast cancer," *IEEE Microwave Magazine*, Vol. 12, No. 7, 78–94, 2011.
9. Shea, J. D., P. Kosmas, S. C. Hagness, and B. D. Van Veen, "Three dimensional microwave imaging of realistic numerical breast phantoms via a multiple-frequency inverse scattering technique," *Medical Physics*, Vol. 37, 4210, 2010.
10. Golnabi, A., P. Meaney, S. Geimer, and K. Paulsen, "Microwave imaging of the breast with incorporated structural information," *Proceedings of SPIE*, Vol. 7626, 76260P, 2010.
11. Gilmore, C., A. Zakaria, S. Pistorius, and J. LoVetri, "Microwave imaging of human forearms: Pilot study and image enhancement," *Journal of Biomedical Imaging*, Vol. 2013, 19, 2013.
12. Fhager, A. and M. Persson, "Using a priori data to improve the reconstruction of small objects in microwave tomography," *IEEE Transactions on Microwave Theory and Techniques*, Vol. 55, No. 11, 2454–2462, 2007.
13. Zakaria, A., A. Baran, and J. LoVetri, "Estimation and use of prior information in FEM-CSI for biomedical microwave tomography," *Antennas and Wireless Propagation Letters*, 1606–1609, 2012.
14. Kurrant, D. and E. Fear, "Technique to decompose nearfield reflection data generated from an object consisting of thin dielectric layers," *IEEE Transactions on Antennas and Propagation*, Vol. 60, No. 8, 3684–3692, 2012.
15. Kurrant, D. J. and E. C. Fear, "Regional estimation of the dielectric properties of inhomogeneous objects using near-field reflection data," *Inverse Problems*, Vol. 28, No. 7, 075001, 2012.
16. Semenov, S. Y. and D. R. Corfield, "Microwave tomography for brain imaging: Feasibility assessment for stroke detection," *International Journal of Antennas and Propagation*, Vol. 2008, 8, 2008.